SUPPLEMENTARY MATERIALS
for
Water-Wave Vortices and Skyrmions

Daria A. Smirnova,[1,2] Franco Nori,[1,3,4] and Konstantin Y. Bliokh[1,5,6]

[1] *Theoretical Quantum Physics Laboratory, Cluster for Pioneering Research, RIKEN, Wako-shi, Saitama 351-0198, Japan*
[2] *Research School of Physics, Australian National University, Canberra, ACT 2601, Australia*
[3] *Center for Quantum Computing (RQC), RIKEN, Wako-shi, Saitama 351-0198, Japan*
[4] *Physics Department, University of Michigan, Ann Arbor, MI 48109-1040, USA*
[5] *Centre of Excellence ENSEMBLE3 Sp. z o.o., 01-919 Warsaw, Poland*
[6] *Donostia International Physics Center (DIPC), Donostia-San Sebastián 20018, Spain*

I. GRAVITY-CAPILLARY WAVES AND FINITE-DEPTH EFFECTS

A. General equations

Here we provide the derivation of Eqs. (1) of the main text for deep-water gravity-capillary waves and consider the finite-depth effects. We start with the standard textbook equations involving the velocity potential $\Phi(x, y, z)$: $\boldsymbol{\mathcal{V}} = \boldsymbol{\nabla}\Phi$ [S1] and restrict ourselves to linear waves, assuming low-amplitude disturbances of the initially flat surface at $z = 0$.

Potential flow of an incompressible non-viscous fluid is described by the Laplace's equation

$$\boldsymbol{\nabla} \cdot \boldsymbol{\mathcal{V}} = \Delta\Phi = 0\,, \tag{S1}$$

with the boundary conditions imposed at the free surface of the liquid and at its finite depth $z = -H$. The kinematic boundary condition for the vertical velocity at the surface yields in the linear approximation:

$$\mathcal{V}_z\bigg|_{z=0} = \frac{\partial \mathcal{Z}}{\partial t} = \frac{\partial \Phi}{\partial z}\bigg|_{z=0}. \tag{S2}$$

Here $\mathcal{Z}(x, y, t)$ is the local vertical displacement of the water surface. At the bottom of the liquid, the no-penetration boundary condition $V_z(z = -H) = 0$ reads

$$\frac{\partial \Phi}{\partial z}\bigg|_{z=-H} = 0\,. \tag{S3}$$

Next, the surface tension at the curved water surface $z = \mathcal{Z}(x, y, t)$ provides the local contribution to the pressure under the surface: $p_{\rm st} = -\alpha\Delta_2\mathcal{Z}$, where α is the surface-tension coefficient and $\Delta_2 = \partial^2/\partial x^2 + \partial^2/\partial y^2$ is the 2D Laplace operator. With this contribution, the linearized Euler equation results in the near-surface ($z = 0$) equation of motion [S1]:

$$\frac{\partial \Phi}{\partial t} = -\left(g - \frac{\alpha}{\rho}\Delta_2\right)\mathcal{Z}\,, \tag{S4}$$

where g is the gravitational acceleration. Applying the time-derivative $\partial/\partial t$ to this equation and using Eq. (S2), we obtain:

$$\left[\frac{\partial^2 \Phi}{\partial t^2} + \left(g - \frac{\alpha}{\rho}\Delta_2\right)\frac{\partial \Phi}{\partial z}\right]_{z=0} = 0\,. \tag{S5}$$

We seek for the plane-wave-like solutions:

$$\Phi = \mathrm{Re}\,\Phi_0(z)\exp(-i\omega t + i\mathbf{k}\cdot\mathbf{r}_2)\,. \tag{S6}$$

Substituting this into Eq. (S1) yields $d^2\Phi_0/dz^2 = k^2\Phi_0$, and using the boundary condition (S3), we obtain

$$\Phi_0(z) = C\cosh\left[k(z+H)\right], \tag{S7}$$

where C is a constant amplitude. Substituting Eqs. (S6) and (S7) into Eq. (S5), we derive the well known dispersion relation for the gravity-capillary waves:

$$\omega^2 = \left[gk + (\alpha/\rho)k^3\right]\tanh(kH)\,. \tag{S8}$$

For $kH > 1$, one can use the deep-water approximation $\tanh(kH) \simeq 1$. For $k \gg \sqrt{g\rho/\alpha}$ the capillary effects dominate, whereas for $k \ll \sqrt{g\rho/\alpha}$ the gravity dominates.

B. Deep-water gravity-capillary waves

We first consider capillary effects in the deep-water approximation. In this case, all monochromatic fields Φ, $\boldsymbol{\mathcal{V}}$, etc. share the same exponential dependence on z: $\propto \exp(kz)$. To derive the equations of motion (1) in the main text, we apply the operator $(\partial/\partial t)\boldsymbol{\nabla}_2$ to Eq. (S4) supplied with relations (S1), (S2), and obtain:

$$\frac{\partial^2 \boldsymbol{\mathcal{V}}_2}{\partial t} = -\left(g - \frac{\alpha}{\rho}\Delta_2\right)\boldsymbol{\nabla}_2\mathcal{V}_z\,. \tag{S9}$$

Next, since all scalar fields are proportional to each other in linear deep-water waves, we can use Eq. (S5) with the substitution $\Phi \to \mathcal{Z}$. Applying operator $(\partial/\partial t)$ to this equation, together with relations (S1), (S2), we obtain:

$$\frac{\partial^2 \mathcal{V}_z}{\partial t} = \left(g - \frac{\alpha}{\rho}\Delta_2\right)\boldsymbol{\nabla}_2\cdot\boldsymbol{\mathcal{V}}_2\,. \tag{S10}$$

Since the Eulerian velocity field is related to the dis-

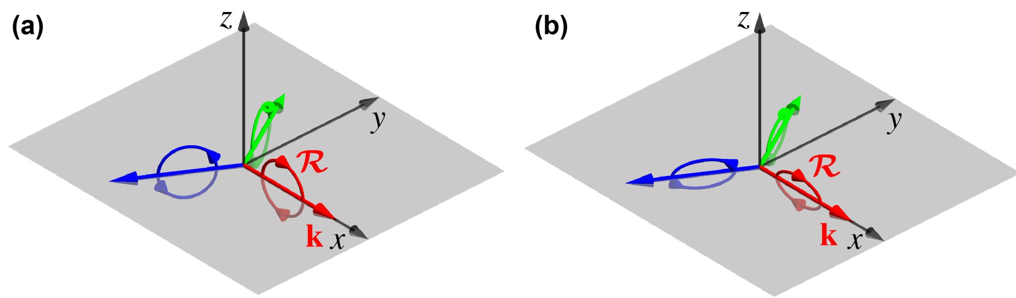

FIG. S1. Effect of finite water depth H on a superposition of monochromatic plane water waves. These plots show three wavevectors $\mathbf{k}$ of interfering plane waves and the corresponding trajectories $\boldsymbol{\mathcal{R}}(t)$ of water-surface particles for each of these plane waves. (a) In the deep-water approximation $kH \gg 1$, the plane-wave water-particle trajectories are circles, whereas (b) in the finite-depth case these are ellipses squeezed vertically by the factor $\varepsilon = \tanh(kH) < 1$. The water-particle trajectories of the resulting interference field can have complex distributions, as shown in the main text, but the deep-water and finite-depth cases (a) and (b) always differ by the same global scaling $\mathcal{Z} \to \varepsilon \mathcal{Z}$.

placement as $\boldsymbol{\mathcal{V}} = \partial \boldsymbol{\mathcal{R}}/\partial t$, the same equations (S9) and (S10) are valid for the displacement field on the water surface. Assuming the monochromatic ansatz $\partial/\partial t \to -i\omega$ and $\boldsymbol{\mathcal{R}} \to \mathbf{R}$, we arrive at Eqs. (1) of the main text:

$$\omega^2 \mathbf{R}_2 = \left(g - \frac{\alpha}{\rho}\Delta_2\right) \boldsymbol{\nabla}_2 Z\,,$$
$$\omega^2 Z = -\left(g - \frac{\alpha}{\rho}\Delta_2\right) \boldsymbol{\nabla}_2 \cdot \mathbf{R}_2\,. \tag{S11}$$

Note that the difference between the capillary-wave and gravity-wave regimes, with different dispersion relations, is inessential for our study. Indeed, the difference in dispersions is important for the evolution of wavepackets (i.e., non-monochromatic waves), but it does not affect the interference of monochromatic waves. This difference only affects the velocity of motion of spatiotemporal vortices in Fig. 3, but does not change this phenomenon qualitatively.

C. Finite-depth effects

We now examine the effects of finite water depth H. Let us consider a single plane wave propagating along the x-axis: $\mathbf{k} \equiv (k_x, k_y) = (k, 0)$. It follows from Eqs. (S6) and (S7) that the vertical and horizontal velocity components trace an ellipse in the (z, x) plane:

$$V_z \propto \sinh[k(z+H)]e^{ikx}\,, \quad V_x \propto i\cosh[k(z+H)]e^{ikx}\,. \tag{S12}$$

In the deep-water limit, this ellipse becomes a circle: $(V_z, V_x) \propto (1, i)$. In the finite-depth case, the ellipse on the $z = 0$ surface is elongated along the x-axis, with the ration of the minor and major semiaxes $\varepsilon = iV_z/V_x = \tanh(kH) < 1$, see Fig. S1.

When we consider a superposition of multiple plane waves with the same frequency, different wavevectors $\mathbf{k}$, and different complex amplitudes, it is easy to see that the effect of the finite depth on the surface motion of water particles is simply the *global scaling of the vertical component of this motion*: $V_z \to \varepsilon V_z$ or $Z \to \varepsilon Z$.

Thus, all the main-text results for monochromatic waves remain valid because this vertical scaling of the vector field $\mathbf{R} = (X, Y, Z) \to (X, Y, \varepsilon Z)$ does not change any topological or angular-momentum properties. Concerning the equations of motion for monochromatic finite-depth gravity-capillary waves, the first equation (S11) remains valid, while the second equation should be modified as follows:

$$\omega^2 \mathbf{R}_2 = \left(g - \frac{\alpha}{\rho}\Delta_2\right) \boldsymbol{\nabla}_2 Z\,,$$
$$\omega^2 Z = -\,\varepsilon^2\left(g - \frac{\alpha}{\rho}\Delta_2\right) \boldsymbol{\nabla}_2 \cdot \mathbf{R}_2\,. \tag{S13}$$

II. VORTICES AND SKYRMIONS IN CLOSED RESERVOIRS

It is possible to experimentally generate and study interference of multiple propagating water wave; see, e.g., the two-wave interference experiment in [S2]. However, such experiments are challenging because of reflections of propagating waves from the boundaries of the reservoir. Therefore, configurations with *standing* waves, which are naturally supported by finite cavities are always preferable.

First, we note that the Bessel-like cylindrical vortices, described in the second section of the main text, can be considered as an interference of multiple standing waves. Indeed, every wavevector $\mathbf{k}$ shown in Fig. 1(b) has its counter-vector $-\mathbf{k}$. Such pairs form standing waves with the same amplitudes but different phases. It is known from the generation of similar surface plasmon-polariton vortices [S3, S4] that such vortices can be generated in a near-circular cavity with a spiral boundary. Similar spiral boundary having radial discontinuity of $2\pi\ell/k$, vertically oscillating in a water tank can generate stationary Bessel-like vortices inside the boundary. Alternatively, a good approximation to such vortices can be provided by a finite

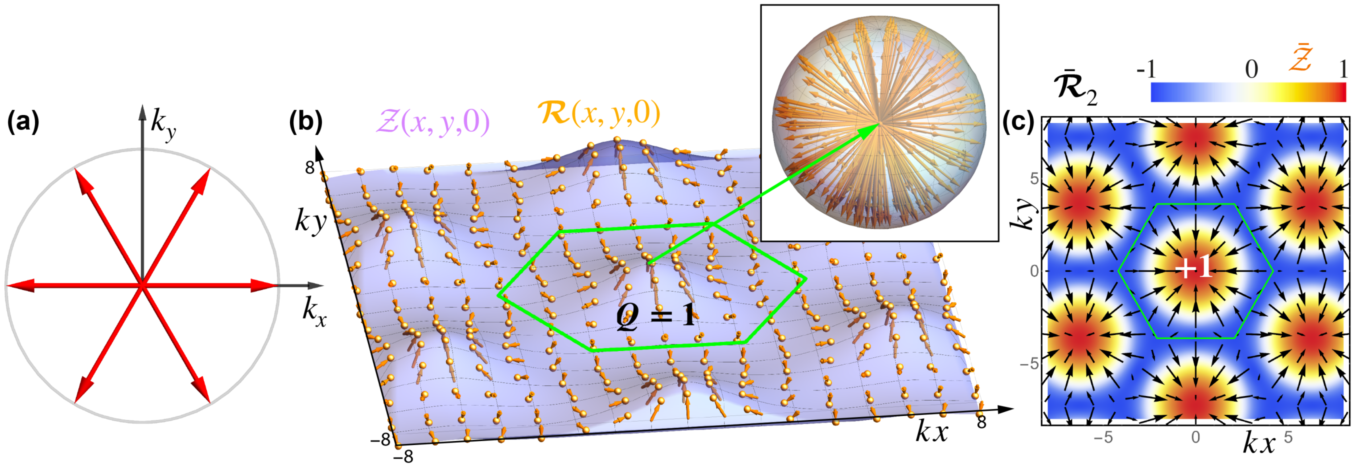

FIG. S2. The hexagonal skyrmion lattice formed by the instantaneous displacement distribution $\boldsymbol{\mathcal{R}}(x, y, 0)$, entirely similar to that in Fig. 2 of the main text, but now produced by the interference of three standing waves (i.e., six propagating waves) with the wavevectors shown in the panel (a).

number $N \gg 1$ of point sources equidistributed along a circle of suitable diameter with the azimuthal phase delay $\ell\varphi$.

Second, in the main text we considered the interference of three propagating waves with different phases, because this simple example exhibits a variety of structures: skyrmions, spin merons, and vortices. However, the same lattice of skyrmions can be generated using the interference of three *standing* (i.e., 6 propagating) waves, with an orientation of $2\pi/3$ relative to each other, Fig. S2. The displacement field is real-valued in this case:

$$\begin{pmatrix} X \\ Y \\ Z \end{pmatrix} \propto A \begin{pmatrix} -\sin kx - \sin\left(\frac{kx}{2}\right)\cos\left(\frac{\sqrt{3}ky}{2}\right) \\ -\sqrt{3}\cos\left(\frac{kx}{2}\right)\sin\left(\frac{\sqrt{3}ky}{2}\right) \\ \cos kx + 2\cos\left(\frac{kx}{2}\right)\cos\left(\frac{\sqrt{3}ky}{2}\right) \end{pmatrix}. \quad \text{(S14)}$$

It coincides, up to the lateral translation, with the real part of the complex field (9) in the main text. Note that vortices and spin merons do not appear in this case (the spin density vanishes identically). This configuration of three standing waves is naturally produced in a closed hexagonal reservoir, entirely similar to experiments with surface plasmon-polaritons [S5], acoustic [S6], and elastic Rayleigh waves [S7].

Thus, water-wave vortices and skyrmions can be readily generated using standing waves in closed reservoirs, akin to experiments with optical or acoustic surface waves and to earlier water-wave experiments [S2, S8–S10] with orthogonal standing waves in square reservoir.

[S1] L. D. Landau and E. M. Lifshitz, *Fluid Mechanics* (Butterworth-Heinemann, Oxford, 1987).

[S2] K. Y. Bliokh, H. Punzmann, H. Xia, F. Nori, and M. Shats, "Field theory spin and momentum in water waves," Sci. Adv. **8**, eabm1295 (2022).

[S3] Y. Gorodetski, A. Niv, V. Kleiner, and E. Hasman, "Observation of the spin-based plasmonic effect in nanoscale structures," Phys. Rev. Lett. **101**, 043903 (2008).

[S4] E. Prinz, M. Hartelt, G. Spektor, M. Orenstein, and M. Aeschlimann, "Orbital angular momentum in nanoplasmonic vortices," ACS Photonics **10**, 340 (2023).

[S5] S. Tsesses, E. Ostrovsky, K. Cohen, B. Gjonaj, N. H. Lindner, and G. Bartal, "Optical skyrmion lattice in evanescent electromagnetic fields," Science **361**, 993 (2018).

[S6] H. Ge, X.-Y. Xu, L. Liu, R. Xu, Z.-K. Lin, S.-Y. Yu, M. Bao, J.-H. Jiang, M.-H. Lu, and Y.-F. Chen, "Observation of acoustic skyrmions," Phys. Rev. Lett. **127**, 144502 (2021).

[S7] L. Cao, S. Wan, Y. Zeng, Y. Zhu, and B. Assouar, "Observation of phononic skyrmions based on hybrid spin of elastic waves," Sci. Adv. **9**, eadf3652 (2023).

[S8] S. V. Filatov, S. A. Aliev, A. A. Levchenko, and D. A. Khramov, "Generation of vortices by gravity waves on a water surface," JETP Lett. **104**, 702 (2016).

[S9] S. V. Filatov, V. M. Parfenyev, S. S. Vergeles, M. Yu. Brazhnikov, A. A. Levchenko, and V. V. Lebedev, "Nonlinear generation of vorticity by surface waves," Phys. Rev. Lett. **116**, 054501 (2016).

[S10] N. Francois, H. Xia, H. Punzmann, P. W. Fontana, and M. Shats, "Wave-based liquid-interface metamaterials," Nat. Commun. **8**, 14325 (2017).